Extended Data

for

Tumor cell p38 inhibition to overcome immunotherapy resistance

Jason J. Luke[1,2,#], Rebekah E. Dadey[1,2], Ryan Augustin[1,2], Sarah Newman[2], Krishna B. Singh[1,2], Rose Doerfler[1,2], Sarah Behr[1], Patrice Lee[3], Brian Isett[1,4], Christopher Deitrick[1,4], Aofei Li[5], Marion Joy[6], Carly Reeder[1,7,8], Katelyn Smith[1], Julie Urban[1], Lorenzo Sellitto[1], Mark Jelinek[9,10], Susan M. Christner[11], Jan H. Beumer[11,12,13], Liza C. Villaruz[1,2], Aditi Kulkarni[1,7,8], Diwakar Davar[1,2], Andrew S. Poklepovic[14,15], Yana Najjar[1,2], Dan P. Zandberg[1], Adam C. Soloff[16], Tullia C. Bruno[1,7], Lazar Vujanović[1,8], Heath D. Skinner[1,17], Robert L. Ferris[1,7,8], Riyue Bao[1,2,#]

[1] Hillman Cancer Center, UPMC, Pittsburgh, PA, USA

[2] Department of Medicine, University of Pittsburgh, Pittsburgh, PA, USA

[3] Pfizer, Inc. Boulder, CO, USA

[4] Cancer Bioinformatics Core, UPMC, Pittsburgh, PA, USA

[5] Department of Pathology, University of Pittsburgh, Pittsburgh, PA, USA

[6] Translational Pathology Imaging Laboratory, UPMC, Pittsburgh, PA, USA

[7] Department of Immunology, University of Pittsburgh, Pittsburgh, PA, USA

[8] Department of Otolaryngology, University of Pittsburgh, Pittsburgh, PA, USA

[9] Department of Biostatistics, University of Pittsburgh, Pittsburgh, PA, USA

[10] Biostatistics Core, UPMC, Pittsburgh, PA, USA

[11] Cancer Therapeutics Program, UPMC Hillman Cancer Center, Pittsburgh, PA, USA

[12] Division of Hematology/Oncology, Department of Medicine, School of Medicine, University of Pittsburgh, Pittsburgh, PA, USA

[13] Department of Pharmaceutical Sciences, School of Pharmacy, Pittsburgh, PA, USA

[14] Departments of Massey Cancer Center, Virginia Commonwealth University, Richmond, Virginia, USA.

[15] Departments of Internal Medicine, Virginia Commonwealth University, Richmond, Virginia, USA.

[16] Department of Cardiothoracic Surgery, University of Pittsburgh, Pittsburgh, PA, USA

[17] Department of Radiation Oncology, University of Pittsburgh, Pittsburgh, PA, USA

[#] To whom correspondence should be addressed: J.J.L. (lukejj@upmc.edu) and R.B. (baor@upmc.edu).

Supplementary Figures

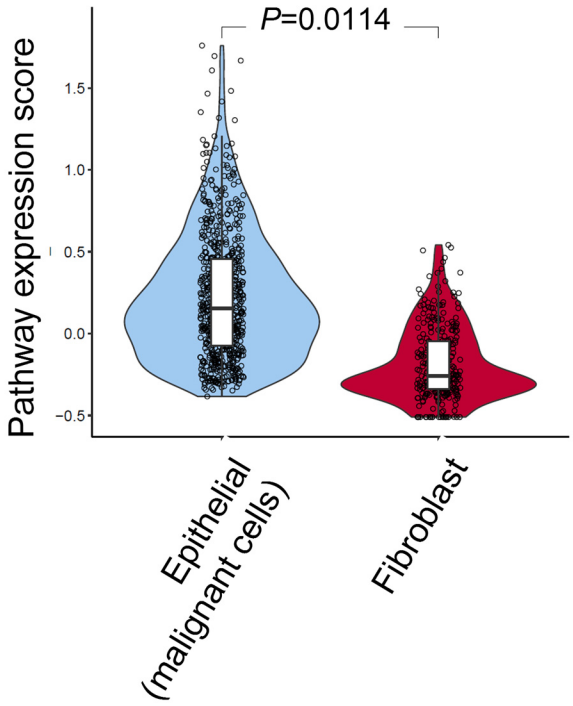

Fig. S1. p38 pathway expression scores in malignant epithelial cells and fibroblasts from HPV-negative HNSCC scRNAseq cohort A (Puram, et al.). P-value was computed by linear mixed-effects models (LMM) with a nested design (patient id as the blocking factor), followed by likelihood ratio test (LRT).

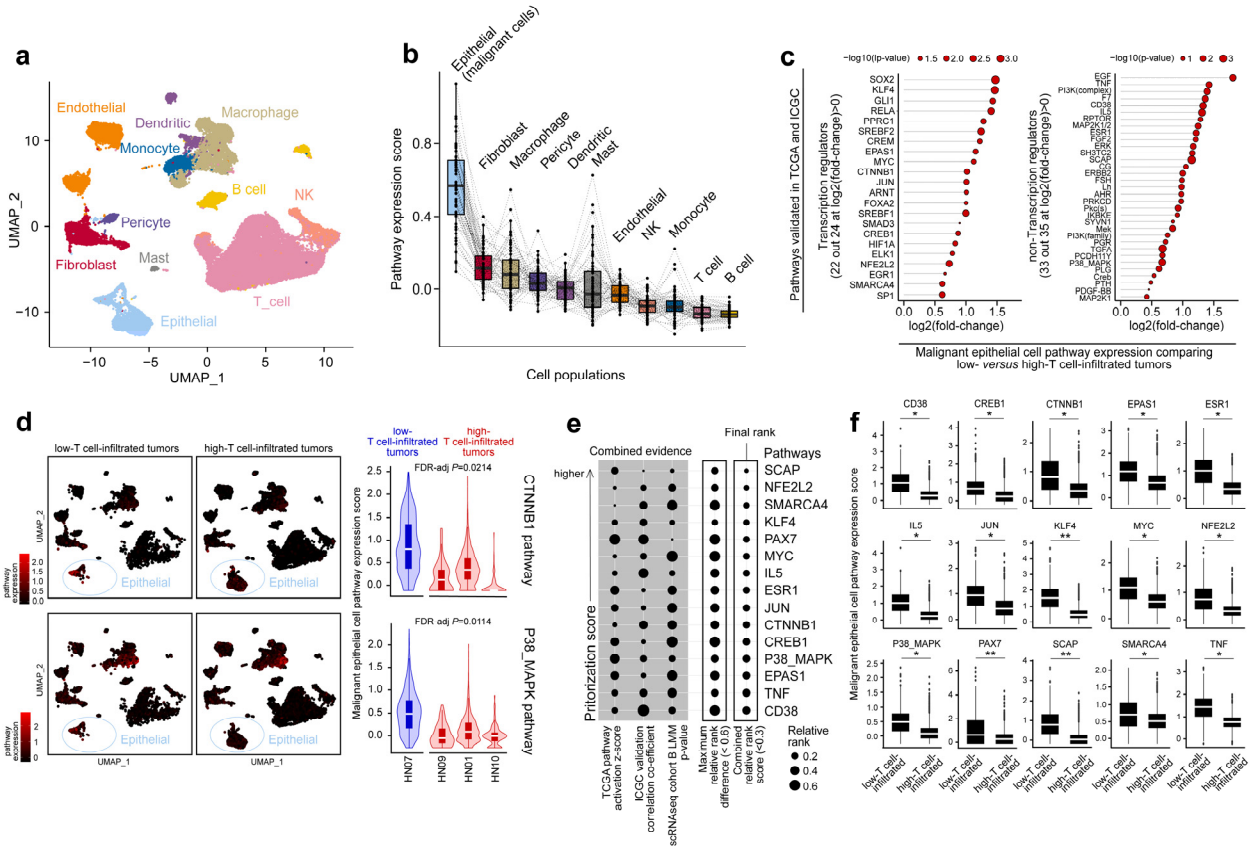

Fig. S2. non-T cell-inflamed phenotype-associated pathways are activated in malignant cells from HPV-negative HNSCC of low T cell infiltration from scRNAseq cohort B (Kurten et al.). (**a**) Distribution of tumor, stroma, and immune cell subsets on UMAP (n=41435 cells from nine tumors). (**b**) Expression of 59 pathways from **Fig. 1d** across cell populations. Pathway scores were computed as the average expression of all genes involved in a pathway. (**c**) 55 out of 59 pathways showed higher expression in 689 malignant epithelial cells of low-T cell-infiltrated relative to 2834 malignant epithelial cells of high-T cell-infiltrated tumors. Bold font represents pathways at FDR 0.10. (**d**) Expression of CTNNB1 pathway and p38 pathway from low- vs high-T cell-infiltrated tumors. Four out of nine tumors with at least 40 malignant epithelial cells per sample were included in analysis. (**e**) 15 pathways that passed prioritization score (combined relative rank) < 0.6 and maximum relative rank difference < 0.3. Six out of 15 pathways overlap with the top pathways from the Puram cohort in **Fig. 2e**. For each of the 59 pathways from **Fig. 1d**, its combined relative rank was computed as the geometric mean of three values: the relative rank in TCGA pathway activation (z-score higher to lower), the relative rank in ICGC anti-correlation with T cell-inflamed expression (coefficient highly to lowly negative), and the relative rank in scRNAseq pathway expression comparing malignant epithelial cells from low-T cell-infiltrated *versus* high-T cell-infiltrated tumors (p-values smaller to

larger). (**f**) Expression of the 15 pathways from **e** Linear mixed-effects model via maximum likelihood was used in **c**, **d** and **f**, with tumor group as the fixed effect and patient id as the random effect. Likelihood ratio test (LRT) was used with the fitted model for computing p-values, followed by BH-FDR correction for multiple comparisons. Denotation: ** FDR-adjusted $P<0.01$, * FDR-adjusted $P<0.05$, otherwise the numbers are shown.

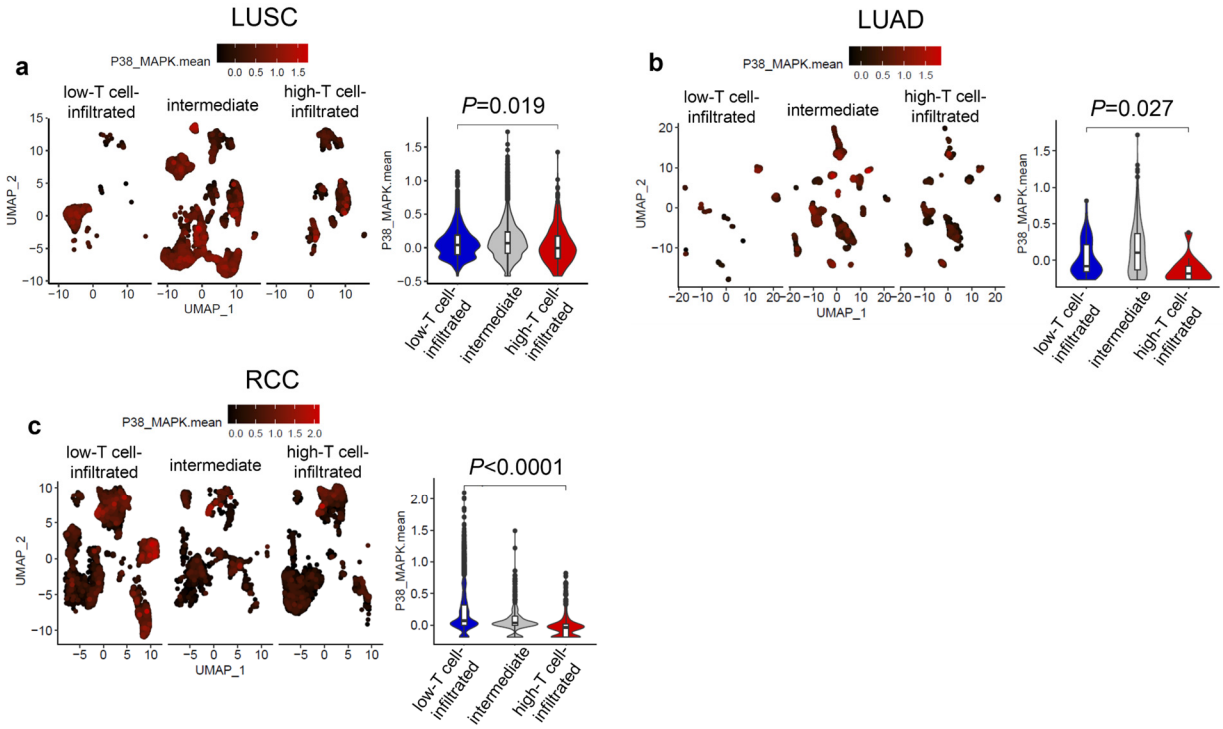

Fig. S3. single-cell analysis of p38/MAPK activation in non-small cell lung cancer and renal cancer. (**a**) lung squamous carcinoma (LUSC). (**b**) lung adenocarcinoma (LUAD). (**c**) renal clear-cell carcinoma (RCC). Two-sided Welch Two Sample t-test was used.

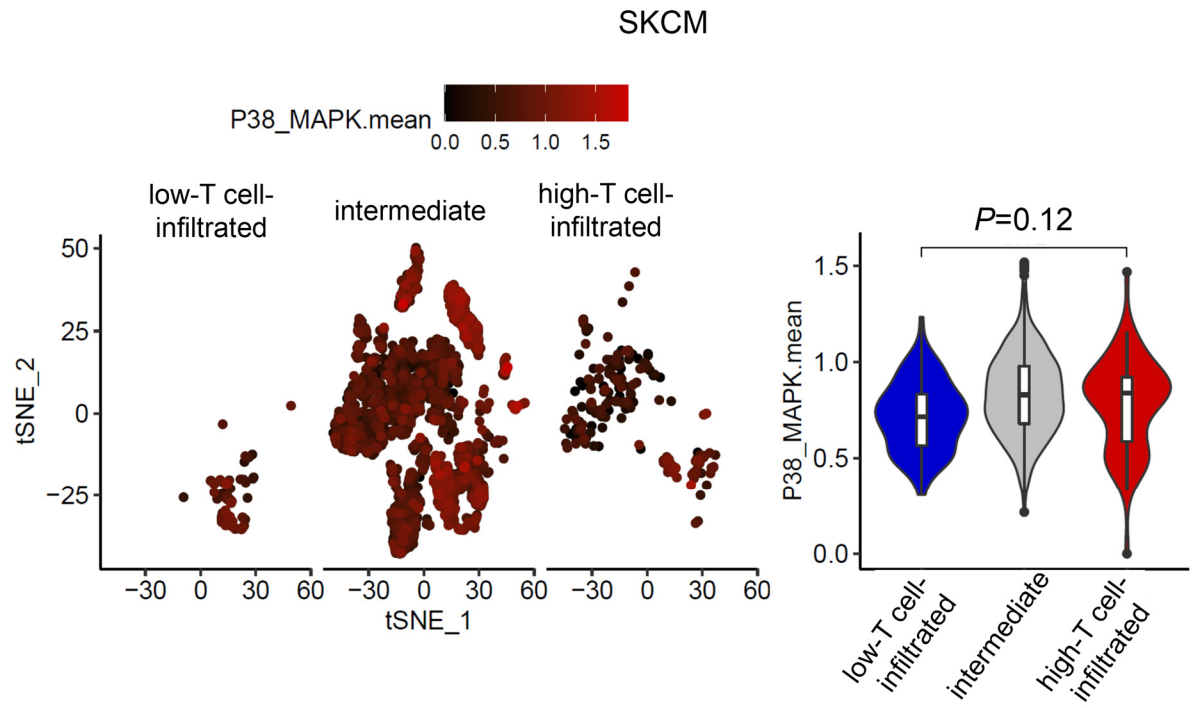

Fig. S4. single-cell analysis of p38/MAPK activation in cutaneous skin melanoma (SKCM). Two-sided Welch Two Sample t-test was used.

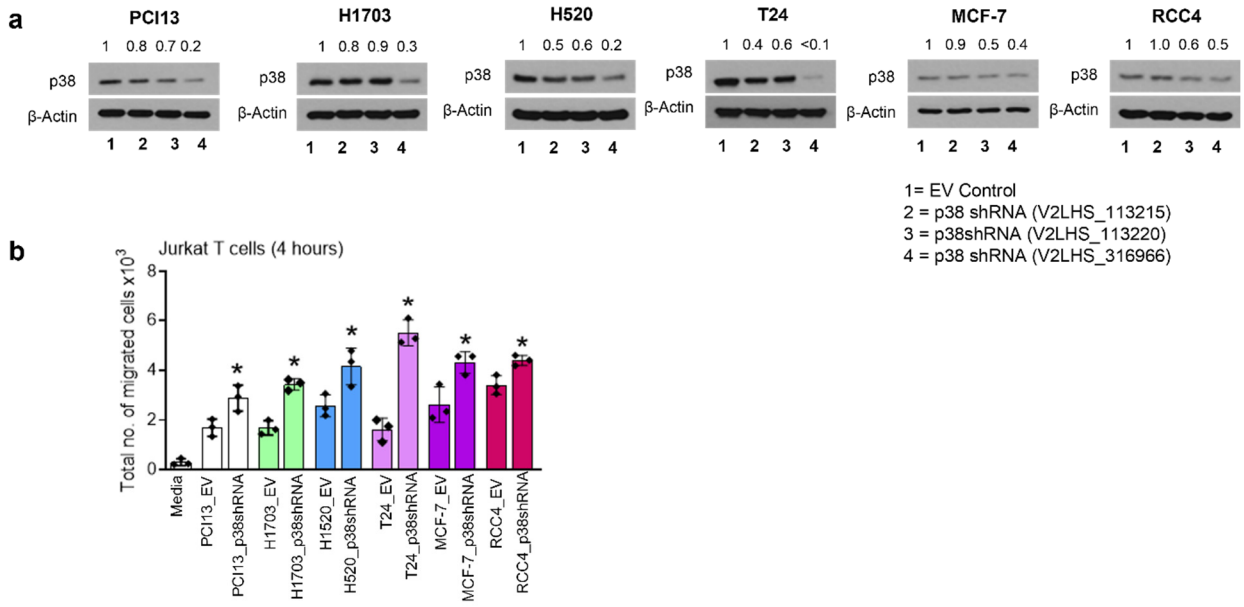

Fig. S5. p38shRNA (*MAPK14*) knockdown mediates T cell attraction in cellular microenvironments. (**a**) Western blot analysis for p38 using lysates from empty vector transfected control cells and p38 shRNA knockdown cells. The numbers above bands represent the change in protein expression levels of p38 relative to EV control. (**b**) Bar plot showing number of migrated T cells in T cell migration assay. Conditioned media from the EV control and corresponding p38 shRNA knockdown cells were used as chemoattractant at the lower chamber of 96-well transwell plate. Serum free media was used as negative control. Each experiment was repeated at least twice in triplicate, and representative data from one such experiment is shown as mean ± SD (n=3 per group). Denotation: * $P < 0.05$ compared with corresponding EV control, and p38 shRNA knockdown cells by two-sided unpaired Student *t*-test.

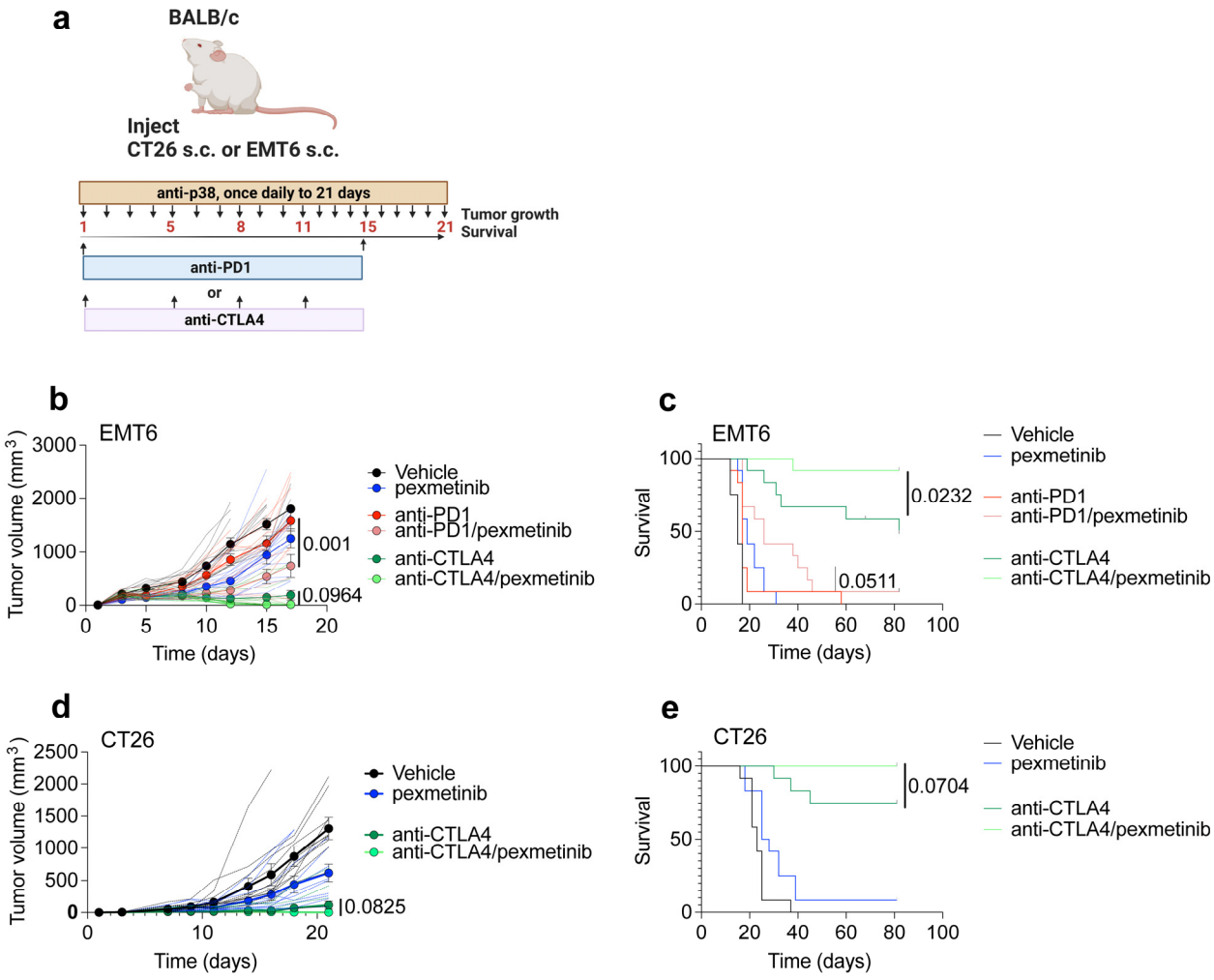

Fig. S6. Pexmetinib (ARRY-614, p38 inhibitor) plus ICI combination therapy shows higher efficacy than monotherapy alone in nonclinical murine models. (**a**) Experimental schema for murine pexmetinib plus anti-PD1/CTLA-4 experiments. **(b-e)** BALB/c females were injected with 5.0 x 10^5 EMT6 cells (n=12 mice/group, 1 experiment) **(b-c)** or 1.0 x 10^5 CT26 cells (n=12 mice/group, 1 experiment) **(d-e)** subcutaneously. Tumors were treated 4 days post tumor cell inoculation with anti-PD1((200 μg)/vehicle on Day 1 and 15 post initial tumor growth phase, or anti-CTLA4 (200 μg)/vehicle on Day 1, 5, 8, and 11 post initial tumor growth phase. Mice receiving pexmetinib were treated orally, once daily for 21 days post initial tumor growth phase. Tumor inhibition growth curves of mice injected with EMT6 **(b)** or CT26 **(d)**, Kaplan Meier survival plots of mice injected with EMT6 **(c)** or CT26 **(e)**. Statistical analysis was determined by 2-way ANOVA adjusted for multiple comparisons (tumor growth) and log rank (Mantel-Cox) test (survival).

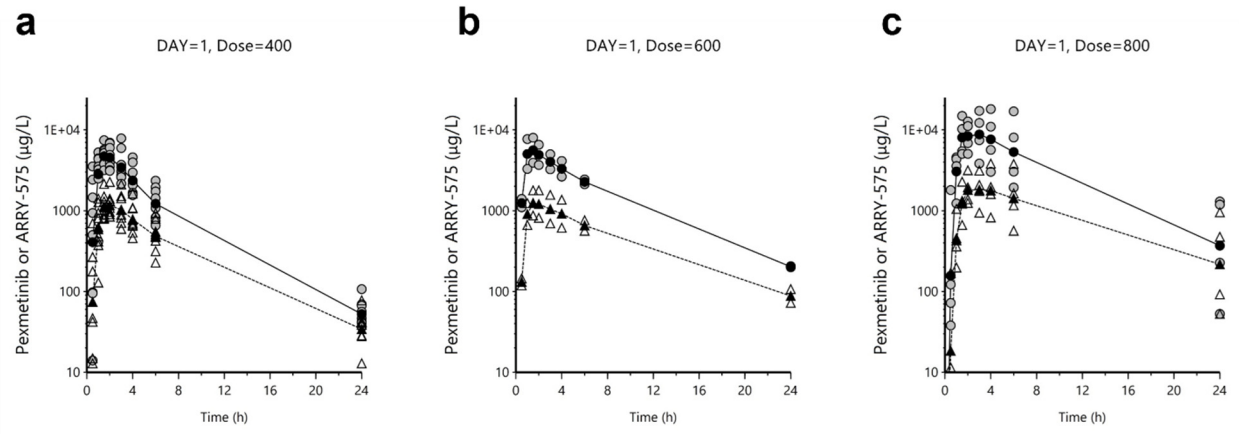

Fig. S7. Pharmacokinetic profiles on day 1 of pexmetinib (grey circles, geometric mean solid circles and line) and metabolite AR00451575 (open triangles, geometric mean solid triangles and dashed line) subset by dose level. (**a**-**c**) Dose = 400, 600, and 800. *n*=15 subjects shown.

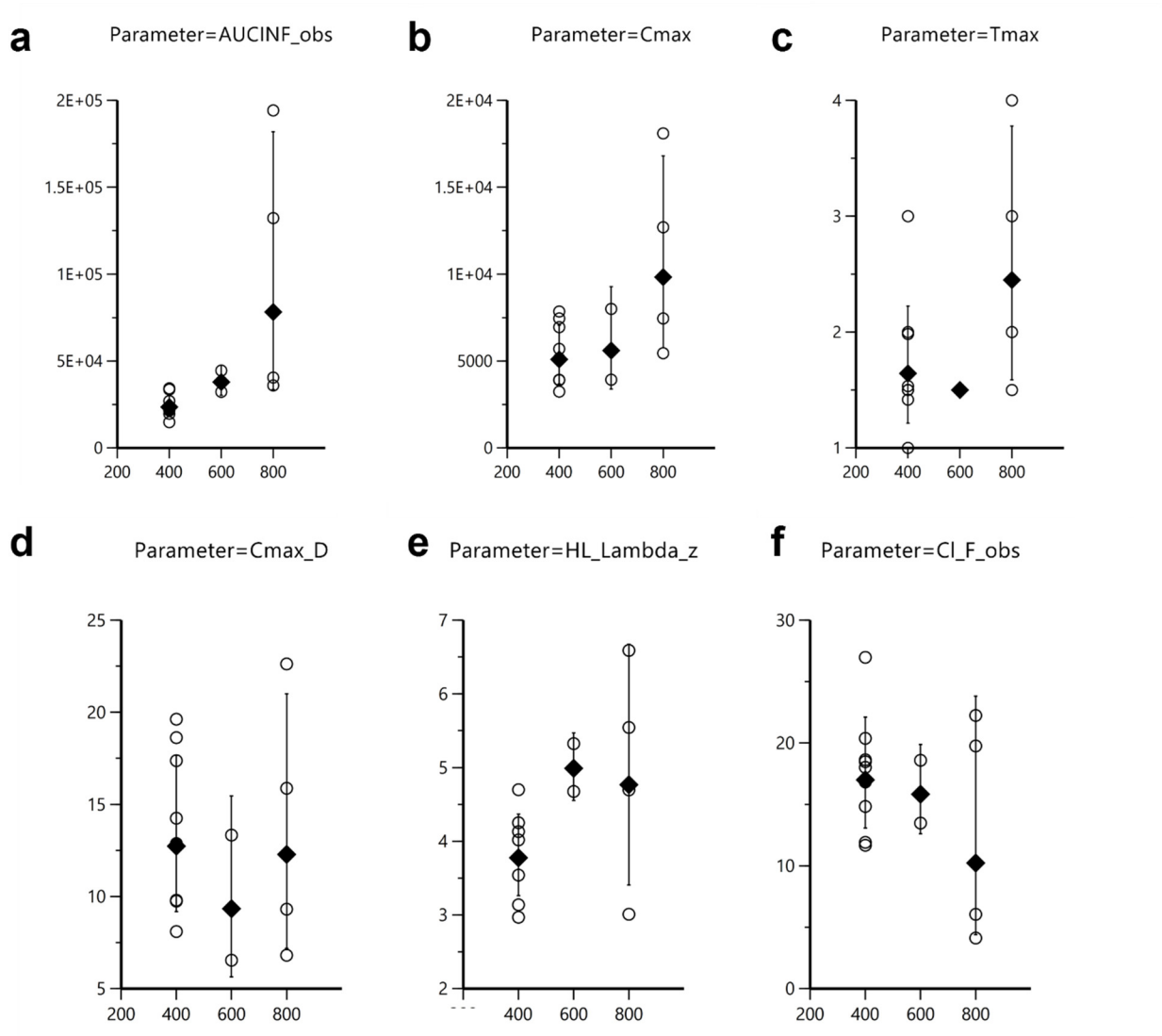

Fig. S8. Pharmacokinetics of pexmetinib as a function of dose. (**a**-**c**) $AUC_{0\text{-}inf}$, C_{max}, and T_{max}. *P*=0.189. (**d**-**f**) dose-normalized C_{max} (**d**, *P*=0.697), increasing half-life (**e**, *P*=0.043), but unaffected clearance (**f**, *P*=0.697) suggesting saturable absorption rate but not total absorption. *n*=15 subjects shown.

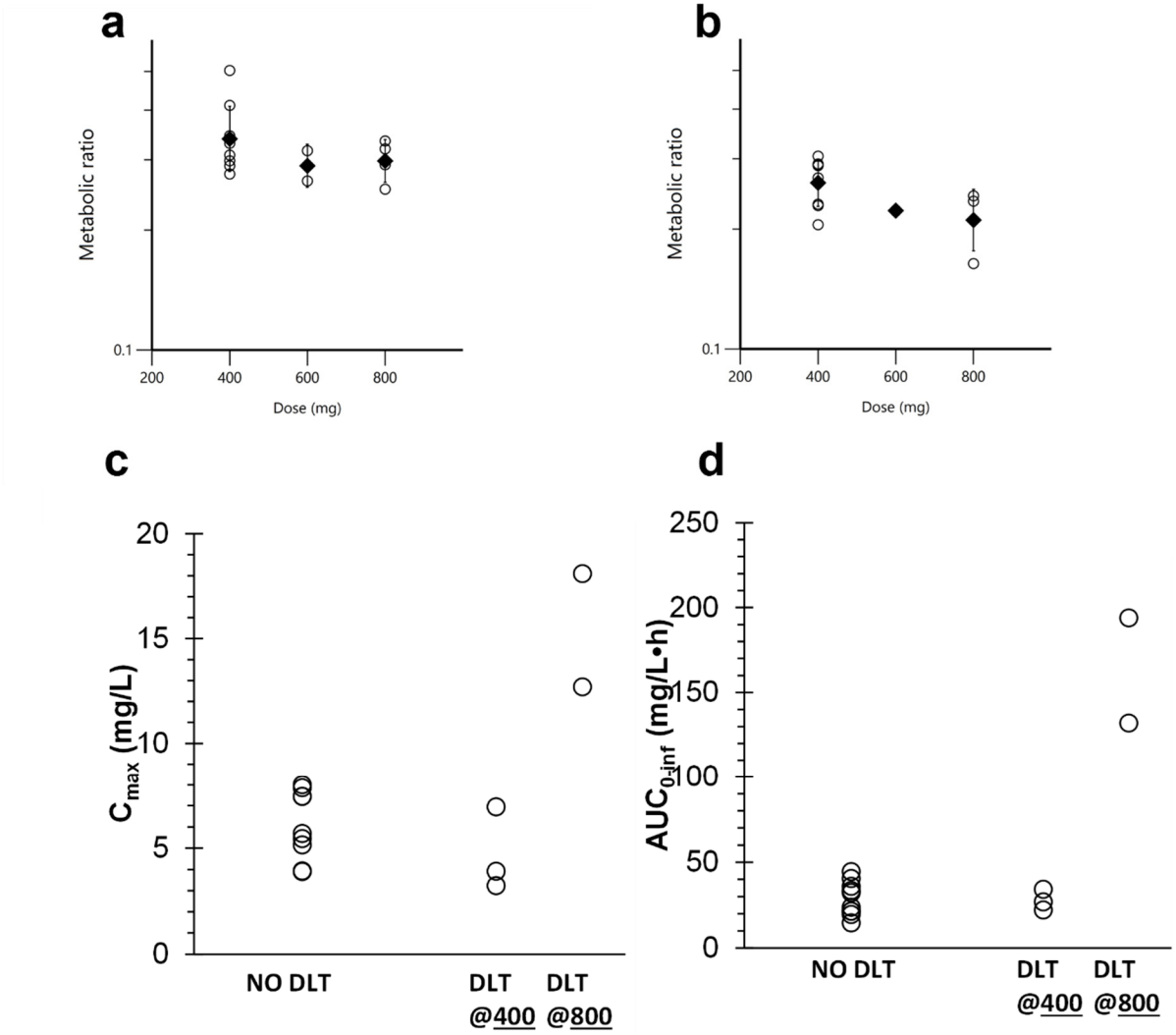

Fig. S9. Metabolic ratio (AR00451575 / pexmetinib) and pharmacokinetics of pexmetinib as a function of dose. (**a**) AUC (*P*=0.238 by Jonckheere-Terpstra). (**b**) C_{max} (*P*=0.043). (**c**-**d**) Exposure-toxicity relationship with higher exposure trending with DLT (**c**, C_{max} *P*=0.355; **d**, AUC *P*=0.058). *n*=15 subjects shown.

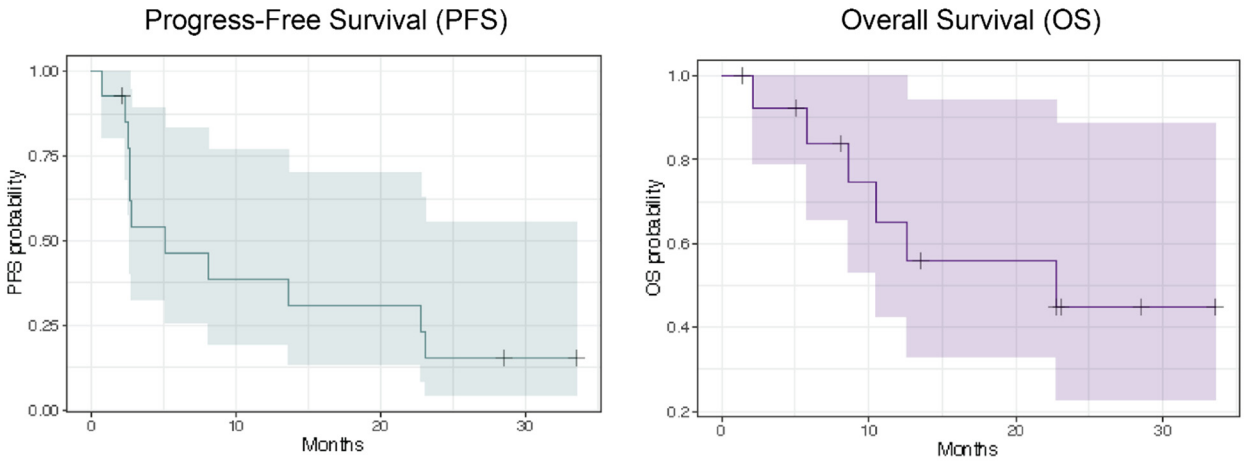

Fig. S10. Kaplan-Meier estimate of progression-free survival (PFS) and overall survival (OS) of subjects treated with pexmetinib plus nivolumab. *n*=14 radiographically evaluable subjects shown.